Synthesis of Carbon Nanotubes (CNTs) from Poultry Litter for Removal of Chromium Cr (VI) from Wastewater

Noor Haleem [a] *, Yousuf Jamal [a, b], Shahid Nawaz Khan [c], Muhammad Anwar Baig [a]

[a] Institute of Environmental Sciences and Engineering (IESE), National University of Sciences and Technology (NUST) Islamabad-44000, Pakistan.

[b] Institute of Chemical Engineering & Technology (ICET), University of the Punjab, Lahore-54590, Pakistan.

[c] Institute of Geographical Information Systems (IGIS), National University of Sciences and Technology (NUST) Islamabad, 44000, Pakistan.

* Corresponding Author: Noor Haleem, nhaleem@iese.nust.edu.pk

Abstract

Pakistan being an agricultural country is raising 146.5 million commercial and domestic poultry birds which generate around 544,831 tons of waste. This waste finds its final disposal in agricultural land as soil fertilizer or disposal site amendment. The uncontrolled use of poultry litter for this purpose results in environmental impacts such as the emission of methane, a greenhouse gas. However, other options like thermochemical conversion of this waste can offer a better solution wherein poultry litter can be used as low-cost carbon sources for the synthesis of Carbon Nanotubes (CNTs). In this study, efforts have been made to utilize this cheap and plenty of available carbon source for synthesis of CNTs in the presence of Ni/Mo/MgO as a catalyst, through pyrolysis. The optimum mole ratio of catalyst (4:0.2:1) was found to yield more carbon product. Furthermore, process parameters such as temperature, time, polymer & catalyst weight were also optimized. The best possible process parameters that resulted (pyrolysis time (12 min), temperature (825°C), and catalyst weight (100 mg) good yield of CNTs . The structure and morphology of produced nanotubes were confirmed through X-ray Diffractometer (X-RD) & Scanning Electron Microscopy (SEM). The environmental application of the nanotubes was tested in synthetic chromium solution in the lab using a batch experiment. Different experimental conditions (pH, adsorbent dosage and contact time) were optimized to enhance the adsorption of Cr (VI) by carbon nanotubes and UV-Visible spectrophotometer was used at 540nm to measure the absorbance of Cr (VI). Results show that up to 81.83% of Cr (VI) removal was achieved by using 8 mg of CNTs at pH 3 with 400 rpm at 180 min of contact time. Thus, it was concluded that

 doi:10.20944/preprints202106.0325.v1

poultry litter can be a useful source for the synthesis of CNTs and thereby removal of Cr (VI) from industrial tanneries wastewater.

Key Words: Poultry litter; Carbon nanotubes; Catalyst; Experimental conditions; Adsorption

1. Introduction

In Pakistan, the poultry sector is one of the vibrant segments of the livestock division. According to 2016-17 statistics, the production of domestic poultry was 85.86 million and commercial poultry was 60.6 million in numbers [1]. Poultry has attained an incredible status in the rural economy and is the second largest industry and mean of livelihood for millions in Pakistan [2]. Asia is the top regional exporter of prepared chicken products, delivering more than 800,000 tons in 2014, while Europe is the main buyer, purchasing more than one million tons in that year [3]. Litter is the organic waste from poultry, mainly consists of feces and urine of chickens. The mixture of poultry manure with spilled feed, feathers, and bedding materials like wood shavings or sawdust are mentioned as poultry litter. The composition and quality of a poultry litter vary with the types of poultry, diet, dietary supplements, storage of litter, and management practices of the poultry farm [4]. The measured data available in the literature regarding the quantity of poultry litter produced per bird in a 42-day production cycle is quietly fluctuating, ranging from 1.5 to 5.7 kg of litter/bird [5]. The average poultry litter production is 3.72 kg/bird. Commonly poultry litter is used in more than one production cycle for chickens. And this helps to reduce the volume of generating beds [3]. The amount of poultry litter generated in a broiler unit depends on the litter (bedding material) management, feed intake, and digestibility [6].

Poultry litter is a rich fertilizer having a wide variety of nutrients important for plant growth has been practically used as organic fertilizer for centuries [7]. Major nutrients specifically N, P, and K while traces nutrients like Cu, Zn, etc. are present in poultry litter [8]. Poultry litter has been also used as a mulching material, it conserves soil moisture and saves the surface feeding roots from drying out in the summer heat [9]. It is also used as a low-cost renewable source for producing activated carbon by burning the litter to at least 700^{o}C resulting in the formation of a lattice-like

Preprints (www.preprints.org) | NOT PEER-REVIEWED | Posted: 11 June 2021 doi:10.20944/preprints202106.0325.v1

carbon particle structure. Activated carbon is used for the adsorption of contaminants in wastewater [10,11], along with this several physico chemical and hydroponic techniques have been reported for metals removal [12-14].

Transition metals reinforced on silica, mesoporous silica, calcium carbonate, zeolites or magnesium oxide is used as catalysts for the growth of CNTs [15]. A large number of catalysts have been studied by improving and changing the structure and properties of CNTs to increase their yield. Various catalysts i.e., Ni, Co, Mo, and Fe have been used for the growth of CNTs. Supported metal catalysts have been formed by using the impregnation method. Keeping in view all parameters related to the chemistry of metal is important while performing the impregnation method for manufacturing of supported metal catalyst [16].

Nanomaterials are progressively used for diverse modern technologies and CNTs are among the most prominent. CNTs are made of graphene sheets of hexagonal structure rolled up into a nanoscale tube. They vary in their lengths up to a million times as compared to their diameter, which down up to is 0.4 nm [17]

CNTs synthesis and its utilization have been studied across the world in the last few years with extraordinary attention. Nowadays, CNTs and their use in different areas have been discussed widely in scientific circles. CNTs have exceptional properties in terms of physical, electrical and mechanical aspects and thus encouraged for new technologies. Other factors that make it different from other materials are its density (nearly half the density of aluminum) crisp stiffness and big surface area [18].

The hydrocarbon sources used for the growth of CNTs include mainly ethylene, methane, and acetylene. While liquid hydrocarbons like benzene, xylene, cyclohexane, and alcohol are also being used as CNTs precursors. Carbon nanotubes can also be generated from solid biomass waste like rice straw [19] and propylene bottles [20].

Studies on the direct growth of Multi-Wall Carbon Nanotubes (MWCNTs) using, in-situ methods of synthesis have been reported, in which carbon containing species were passed over a transition metal alloy that acts as a catalyst. The synthesis of the catalyst, however, be very tedious, lengthy, and un-economical which may increase the cost of the MWCNTs. In recent years, magnetic separation techniques have gradually become the focus of scientist's concern

Preprints (www.preprints.org) | NOT PEER-REVIEWED | Posted: 11 June 2021 doi:10.20944/preprints202106.0325.v1

[21]. It has been applied in many research fields, including medicine, analytical chemistry, cell biology, and environmental engineering. The synthesized magnetic CNTs can be well dispersed in water and easily removed from the medium with the help of a magnet[22]. Removal of inorganic, heavy metals and organic contaminants using biochar[23] and magnetic CNTs [24] as an adsorbent has been reported.

In this work, there were two objectives of this study first to use poultry litter as a carbon source for the production of CNTs over Ni/Mo/MgO catalyst. Response Surface Methodology (RSM) was used to optimize the parameters (like temperature, time, and weight of the catalyst) both for catalyst preparation and growth of CNTs. The second objective of the study was to examine the adsorption behavior of CNTs for the Cr (VI) adsorption. Effect of parameters, such as system pH, adsorbent dosage, and adsorbent contact time were investigated. Effect of pH on removal of Cr (VI) and Pb (II) & Cd (II) was studied comparatively.

2. Materials and method

Commercial poultry units in Islamabad, Pakistan were reached for the collection of poultry litter. Fresh litter was collected since the bird's flock was just removed from the poultry farms. Litter was then transported to the Institute of Environmental Sciences and Engineering (IESE). The bedding material was constituted of sawdust, no medicine was given to the birds during the growth phase. The initial poultry litter sample of 3kg was kept in closed bags. For the synthesis of catalyst, Nickel Nitrate hexahydrate ($Ni(NO_3)_2 \cdot 6H_2O$), Ammonium Molybdate tetrahydrate ($(NH_4)_6Mo_7O_{24} \cdot 4H_2O$), Magnesium nitrate hexahydrate ($Mg(NO_3)_2.6H_2O$), Citric acid, Hydrochloric Acid (HCl), Sodium Hydroxide (NaOH) & Ethanol were purchased from Sigma Aldrich. All chemicals were of analytical grade and used as received. In all the experimental run distilled water was used.

2.1 Synthesis of Catalyst

The wet impregnation method was used for the synthesis of catalysts. The solution of 116.28g of $Ni(NO_3)_2 \cdot 6H_2O$, 24.71g of $(NH_4)_6Mo_7O_{24} \cdot 4H_2O$ and 25.64g of $Mg(NO_3)_2$ 6H2O was taken in 200ml distilled water and stirred for 1hour on a magnetic hot plate. The mixture was heated to 90^{o}C up to 1hour after the addition of two grams of anhydrous citric acid. The resultant mixture was left on a hot plate for evaporation. The viscous slurry was found which was oven-dried at

Preprints (www.preprints.org) | NOT PEER-REVIEWED | Posted: 11 June 2021 doi:10.20944/preprints202106.0325.v1

120°C for 12 hr. The material was ground in fine powder form and calcination in the furnace of tube-like structure at 600°C for 2 h (10° rise/min) [25].

2.2 Synthesis of CNTs

The raw material used for the synthesis of CNTs was poultry litter. Litter was dried in the oven at 120°C for 3 hrs., and ground. 4g of poultry litter was then mixed manually with 2-8mg of catalyst, the mixture was placed in a porcelain boat (volume 80 ml) and then combusted in an electrically heated tube furnace at 700-950°C in a continuous flow of helium gas to provide an inert atmosphere. The porcelain boats were removed after 12 minutes from the tube furnace. During the decomposition of organic compounds, carbon molecules are deposited on the nickel catalysts placed on magnesium oxide as supporting material. In reported literature, the synthesis is carried out within the temperature range of 750–850°C [26].

Following equation (Eq-1) was used to calculate the yield of CNTs.

$$\text{yield} = \frac{m1-m2}{m1} \times 100 \quad (1)$$

Where $m_{1=}$ weight of the as-prepared product and m_2= weight of the catalyst

2.3 Process parameter optimization with Response Surface Methodology

Response Surface Methodology (RSM) with box–behnken design was used to maximize the yield of CNTs by optimization of process parameters. In contrast to conventional methods, the interaction between processes variables were determined by statistical technique the response surface methodology. A 2-level half factorial design with three central points was preferred for the optimization of CNTs production. The optimized parameters were (a) Reaction Time (b) Reaction Temperature and (c) Catalyst concentration. Fifteen experimental runs for the synthesis of CNTs sample are determined by the statistical software. The response for each run based on the yield was further statistically analyzed to find out the optimum reaction conditions [27]

2.4 Purification of CNTs

Impurities like residual catalyst and amorphous carbon are necessary to remove from CNTs. This requires chemical and thermal treatment. Catalyst particles were removed by an ultra-sonication process in which 37% concentrated hydrochloric acid was used and stirred for 2 hr. on a

Preprints (www.preprints.org) | NOT PEER-REVIEWED | Posted: 11 June 2021 doi:10.20944/preprints202106.0325.v1

magnetic hot plate. The resultant mixture was filtered by vacuum after dilution with deionized water. Distilled water is used to neutralize the pH of the solid carbon product. Oxidation of CNTs done in a tube furnace at a temperature of 400◦C for a duration of 2 hr., following the method explained by Vivekchand et al. [28].

2.5 Functionalization of CNT

A solution of 200 ml of 6.0M HNO_3 (70 %) was prepared and 0.7g MWCNT was spread in this solution by dispersion method. An ultrasound bath was used for 20 min to maintain the dispersion process. The magnetic stirring of dispersion was done for 12 hr. The period under nitric acid reflux under different temperatures ranges 50, 70, 90 and 110^{o}C. The dispersion was cooled down at room temperature after removing it from the hot plate after 12 hours of treatment. Centrifugation of dispersion was done at 4000 rpm for 10 min. This process separates the supernatant from the mixture by sediment solid residues. The supernatant was filtered under vacuum by using 0.2 um acetate membrane filter. Distilled water was used to wash the solid residue to remove extra nitric acid from the sample. This washing process continued until the pH of the filtrate became neutral. Finally, MWCNTs were dried for further analysis [29].

2.6 Adsorption of Cr (VI)

The Cr (VI) stock solution of 1000 mg L^{-1} was prepared by dissolving 0.2829 g of potassium dichromate ($K2Cr_2O_7$) in 100 mL distilled water. Several solutions with different concentrations of Cr (VI) were prepared by dilution of the stock solution with distilled water. Adsorption studies were carried out by mixing 2, 4, 6 and 8 mg of MWCNTs with 50 mL Cr (VI) solutions of 100ppm in a 100 mL volumetric flask. The solutions were agitated at 500 rpm over different contact time (30, 60, 90, 120, 150, 180 and 210 min). The pH values of Cr (VI) solutions were adjusted to 2.0 – 7.0 by using 1.0M HCl and 1.0M NaOH solution [30].

The effect of adsorbent dosage was determined and pH value of 3 and the initial Cr (VI) concentrations in the solutions were used. An acetate membrane filter of 0.2 um thickness was selected to separate the aqueous phase. UV-Visible spectrophotometer was run to find out the concentration of Cr (VI) in the filtrate solution.

Following equation (Eq-2) was used to find out the adsorption efficiency (E).

Preprints (www.preprints.org) | NOT PEER-REVIEWED | Posted: 11 June 2021 doi:10.20944/preprints202106.0325.v1

$$E = \frac{Co-Ce}{Co} \times 100 \_\_\_\_\_ (2)$$

Where Co is the initial concentrations and Ce is the initial equilibrium of Cr (VI) respectively.

2.7 Characterizations

2.7.1 X-ray Diffraction

To obtain X-Ray diffraction patterns of the catalyst X-Ray diffractometer (Theta/Theta STOE Jeol Germany) was used. Samples were prepared by pressing the powders between two glass slides into a flattened sheet. Radiation source CuK was used for taking X-ray patterns and 40 kV and 40 mA was supplied to the X-ray generator. The patterns were recorded at 2θ from 20^{o} to 70^{o}.

2.7.2 Scanning Electron Microscopy (SEM)

SEM (Jeol JSM-6490A, Japan Analytical scanning electron microscope) was used to study the surface morphologies of the samples. Samples were coated with a thin layer of conducting material (gold) and were imaged at ×20,000, ×35,000, and 75,000 magnifications, the accelerating voltage was 10–15 kV. A focused, high beam of electrons was interacted with the surface of the sample and generated secondary electron, backscattered electron, and characteristic X-rays signals. These signals were perceived by the detector and images were displayed on the cathode ray tube screen [31].

2.7.3 Transmission Electron Microscopy (TEM)

The sample was characterized using a Jeol JEM-100cx transmission electron microscope with an accelerating voltage of 20 kV. The prepared sample was first sonicated in ethanol for 5 min at room temperature and then a drop of dispersion was deposited on a Cu/Rh grid covered with a vinyl polymer (formvar), and the grid was dried overnight under vacuum [32].

2.7.4 Raman Spectroscopy

Raman spectroscopy of the synthesized CNTs was performed using Raman Spectrophotometer uRaman-532 TEC- Ci Technospex in ambient conditions. The spectrum was recorded using an incident laser having an excitation wavelength of 532 nm and samples were exposed for 60 s.

Preprints (www.preprints.org) | NOT PEER-REVIEWED | Posted: 11 June 2021 doi:10.20944/preprints202106.0325.v1

3. Results and Discussion

3.1 Initial analysis of poultry litter

3.1.1 Moisture content

moisture content (w /w%) of the poultry litter (PL) was determined as the weight loss of about 78.54g of sample after drying in oven at 105ºC for 8 h. Total moisture content of raw material was found 60.73% as shown in table.1.

Table. 1. Moisture content of poultry litter.

Sr. No	Weight of PL before drying (W2) (gm)	Weight of PL after drying (W1) (gm)	Moisture content (%)
1.	200	89.64	55.18
2.	200	42.28	78.86
3.	200	103.7	48.5

$$M = \frac{W2 - W1}{W2} \times 100 \_\_\_\_\_ (1)$$

Average of the above dry weight =78.54. Putting this valve in above eq.1

$$M = \frac{200 - 78.54}{200} \times 100 = 60.73\% \_\_\_\_\_ (2)$$

3.1.2 Elemental analysis

Spectroscopic method (section 3.7.3) was used to determine elemental concentrations in poultry litter as shown in figure 1. Analysis of the composition of poultry litter is shown in table 2. Concentrations of C, N, P, O, CI, Na, Ca, Mg, S and Si were found in PL sample without bedding material (not mixed with bedding material).

Preprints (www.preprints.org) | NOT PEER-REVIEWED | Posted: 11 June 2021 doi:10.20944/preprints202106.0325.v1

Table. 2. Elemental analysis of poultry litter.

Elements	C	N	O	Na	Mg	Si	S	Cl	K	Ca
Conc.	65.17	1.55	18.77	0.70	0.50	0.04	0.08	0.72	1.71	0.98

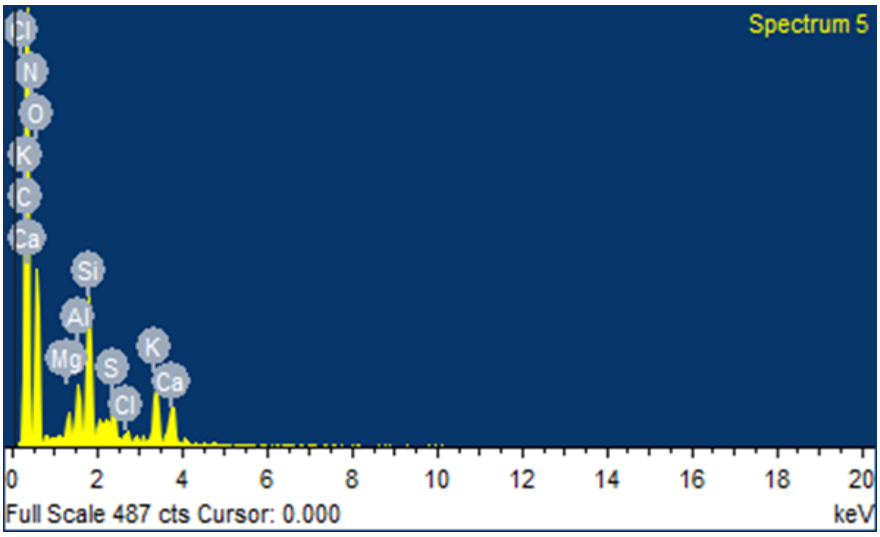

Figure 1. EDS of poultry litter through SEM.

3.2 Optimization of mole ratio of catalyst precursors

To study the effect of Ni/Mo mole ratio on the carbon yield, Response Surface Methodology (RSM) was adopted. The effects of each variable (Ni/Mo/MgO mole ratio) on the dependent variable (carbon yield) were subjected to regression analysis. Multiple linear regression was used to explain the association between one continuous dependent variable (Carbon yield %) and three independent variables (concentration of Ni, Mo, and MgO). To verify the effect of a catalyst on the carbon yield, various concentrations of Ni, Mo and MgO were studied as shown in Table. 3. For optimization of a process parameter, 15 experimental runs were carried out.

Table 3. Optimization of Ni/Mo/MgO concentrations in the catalyst.

Preprints (www.preprints.org) | NOT PEER-REVIEWED | Posted: 11 June 2021 doi:10.20944/preprints202106.0325.v1

Run	A: Nickel (Mol)	B: Molybdenum (Mol)	C: Magnesium oxide (Mol)	Carbon yield (%)
1.	2.00	0.20	2.00	24
2.	2.00	0.60	2.00	21
3.	2.00	0.40	3.00	24
4.	2.00	0.40	1.00	25
5.	4.00	0.40	2.00	39
6.	4.00	0.60	1.00	40
7.	4.00	0.20	3.00	43
8.	4.00	0.40	2.00	38
9.	4.00	0.40	2.00	38
10.	4.00	0.60	3.00	35
11.	4.00	0.20	1.00	44
12.	6.00	0.20	2.00	37
13.	6.00	0.60	2.00	32
14.	6.00	0.60	3.00	32
15.	6.00	0.40	1.00	39

Table 4 explains the response of carbon yield as a function of Ni/Mo mole ratio as a result of analysis of variance (ANOVA). It was observed that the suitable model to study the response of carbon yield was the quadratic model. From the F-value, P-value, and correlation coefficient (R^2) of the model, the adequacy of the model was confirmed. The smaller the value of P indicates that the coefficient is very important. In this model F-value of 117.97 and $P < 0.0001$ confirms that the model was significant. The R^2 value of 0.9953 indicates the fitness of the quadratic model [27,33].

Table 4. ANOVA for Box–Behnken design for carbon yield as a function of different mole ratios of catalyst precursors.

Source	**Sum of Squares**	**df**	**Mean Square**	**F-value**	**p-value**	
Model	763.34	9	84.82	117.97	< 0.0001	significant
A-Ni	277.32	1	277.32	385.72	< 0.0001	
B-Mo	49.16	1	49.16	68.38	0.0004	
C-Mg	11.93	1	11.93	16.59	0.0096	
AB	0.6131	1	0.6131	0.8528	0.3981	
AC	1.08	1	1.08	1.51	0.2743	
BC	3.30	1	3.30	4.59	0.0851	
A^2	335.36	1	335.36	466.45	< 0.0001	
B^2	0.0000	1	0.0000	0.0000	0.9959	

Preprints (www.preprints.org) | NOT PEER-REVIEWED | Posted: 11 June 2021 doi:10.20944/preprints202106.0325.v1

C^2	18.96	1	18.96	26.37	0.0037	
Residual	3.59	5	0.7189			
Lack of Fit	2.93	3	0.9760	2.93	0.2649	not significant
Pure Error	0.6667	2	0.3333			
Cor Total	766.93	14				

R^2 = 0.9953; Adjusted R^2 = 0.9869; Predicted R^2 = 0.9287

Carbon Yield = -3.60000+23.45066Ni +0.328947Mo -7.59868 Mg -0.947368Ni * Mo -0.288158Ni * Mg -4.39474 Mo * Mg -2.42368 Ni^2 +0.065789 Mo^2 +2.30526 Mg^2_____ (3)

The equation (3) in terms of actual factors was used to make predictions about the response for given levels of each factor as shown in figure 2. The three-dimensional response of the catalytic activity of Ni, Mo and MgO over the carbon yield are shown in figure 3.

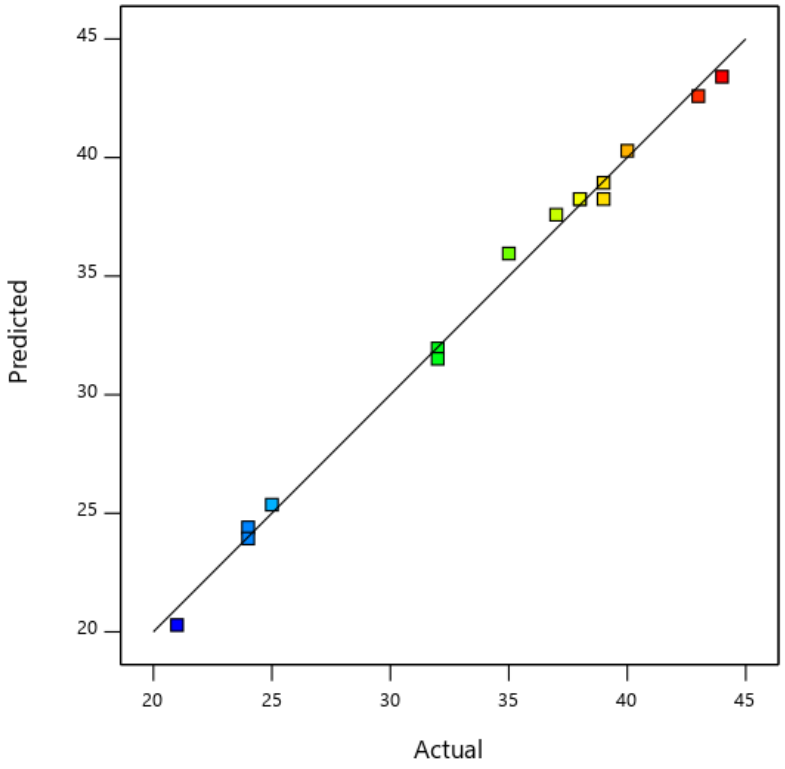

Figure 2. Correlation between experimental and predicted yield of carbon product derived from RSM model.

Preprints (www.preprints.org) | NOT PEER-REVIEWED | Posted: 11 June 2021 doi:10.20944/preprints202106.0325.v1

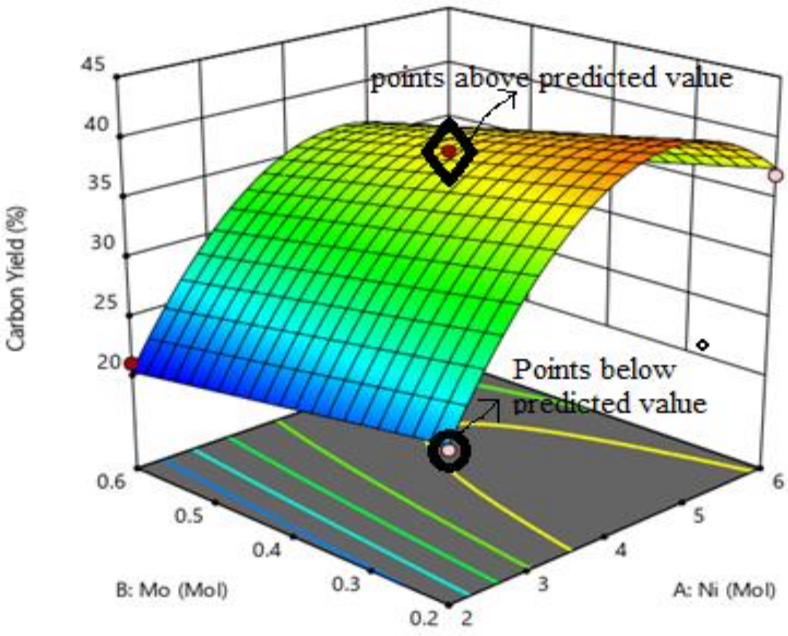

Figure 3. Three-dimensional response plot showing catalytic activity of Ni, Mo and MgO over the carbon yield.

3.3 Statistical analysis and modeling for CNTs growth

The preliminary detection of levels of the process parameters is necessary to carry out. Therefore, optimization was done using trial experiments. To optimize the process parameters, a full factorial design method and several runs were required. In this study, we have performed various initial trial runs based on the summary of results reported by [34]. In all experimental runs, it was observed that less than 12 min of pyrolysis time leads to partial combustion of poultry waste while greater than 20 min leads to the rapid oxidation of CNTs as shown in table.5. CNTs growth was not seen at less than 700˚C and rapid combustion of raw material and oxidation of CNTs was observed at above 900ºC. The highest and lowest values for weight of poultry waste and catalyst are selected based on the volume of porcelain boat used in our experiments.

Preprints (www.preprints.org) | NOT PEER-REVIEWED | Posted: 11 June 2021 doi:10.20944/preprints202106.0325.v1

Table 5. Optimization of process parameters for CNTs growth.

Run	A: Temperature (°C)	B: Time (min)	C: Catalyst weight (mg)	D: Carbon yield (%)
1.	700.00	12.50	80.00	13.24
2.	700.00	12.50	120.00	13.85
3.	700.00	5.00	100.00	14.12
4.	700.00	20.00	100.00	15.51
5.	825.00	20.00	80.00	30.37
6.	825.00	5.00	80.00	30.86
7.	825.00	20.00	120.00	31.02
8.	825.00	5.00	120.00	32.1
9.	825.00	12.50	100.00	44.04
10.	825.00	12.50	100.00	44.38
11.	825.00	12.50	100.00	44.41
12.	950.00	20.00	100.00	16.7
13.	950.00	12.50	80.00	16.72
14.	950.00	12.50	120.00	17.12
15.	950.00	5.00	100.00	18.32

To optimize the response when it is influenced by different parameters, response surface methodology (RSM) was used. The RSM three levels and three variable experimental designs of Box–Behnken were adopted, and 15 experimental runs were carried out to study the effect of the different variables on the carbon yield. Correlation between experimental and predicted yield of carbon product over different variables are shown in figure 4. Reaction temperature (700–950°C), poultry litter weight (2–4g), catalyst weight (80–120 mg), and reaction time (5–20 min) were chosen for the optimization in terms of maximum yield of the carbon product. The optimized values for the synthesis of catalyst (Ni/Mo/MgO) with moles of Ni, Mo, and MgO for growth of CNTs were 4: 0.2:1. Three-dimensional response showing the effect of variables over the carbon yield are shown in figure 5. The effects of different process parameters as an independent variable on the carbon yield are shown in table.6 are subjected to regression analysis and the eq-4 in terms of the actual factors is obtained.

Carbon Yield = -1129.58015 +2.34585 Temperature +3.45479 Time +3.57753 Catalyst Weight

-0.000803 Temperature * Time -0.000021Temprature * Catalyst Weight -0.000983 Time * Catalyst Weight -0.001407 Temprature^2 -0.108970 Time^2-0.017649 Catalyst Weight^2 _____(eq. 4)

Preprints (www.preprints.org) | NOT PEER-REVIEWED | Posted: 11 June 2021 doi:10.20944/preprints202106.0325.v1

The equation in terms of actual factors can be used to make predictions about the response for given levels of each factor. Based on the model fitting test and regression analysis an appropriate model was selected to sort out all possible interactions of selected factors with a response function.

$$\mathbf{Y = ao \sum_{i=1}^{4} aixi + \sum_{i=1}^{4} aiix2i + \sum_{i=1}^{4} aijxixj} \quad (5)$$

Where Y = Response

a_0 = Constant coefficient

a_i, a_{ii}, and a_{ij} = are the coefficients predicted by regression for linear, quadratic, and cross-product effects of X_1, X_2, and X_3 respectively.

In this study the variables X_1, X_2 and X_3 are assigned for reaction temperature [A], reaction time [B], catalyst weight [C] and reaction time [35].

Table 6. ANOVA of Box–Behnken design for carbon yield as a function of different process parameters.

Source	**Sum of Squares**	**Df**	**Mean Square**	**F-value**	**p-value**	
Model	1975.25	9	219.47	1722.93	< 0.0001	significant
A-Temperature	18.42	1	18.42	144.62	< 0.0001	
B-Time	0.4050	1	0.4050	3.18	0.1347	
C-Catalyst Weight	1.05	1	1.05	8.25	0.0349	
AB	2.27	1	2.27	17.78	0.0084	
AC	0.0110	1	0.0110	0.0865	0.7804	
BC	0.0870	1	0.0870	0.6832	0.4461	
A^2	1784.57	1	1784.57	14009.47	< 0.0001	
B^2	138.73	1	138.73	1089.05	< 0.0001	
C^2	184.02	1	184.02	1444.59	< 0.0001	
Residual	0.6369	5	0.1274			

Preprints (www.preprints.org) | NOT PEER-REVIEWED | Posted: 11 June 2021 doi:10.20944/preprints202106.0325.v1

Lack of Fit	0.5524	3	0.1841	4.36	0.1922	not significant
Pure Error	0.0845	2	0.0422			
Cor Total	1975.89	14				

R^2 =0.9997; Adjusted R^2= 0.9991; Predicted R^2 = 0.9954; Adeq. Precision = 106.2977

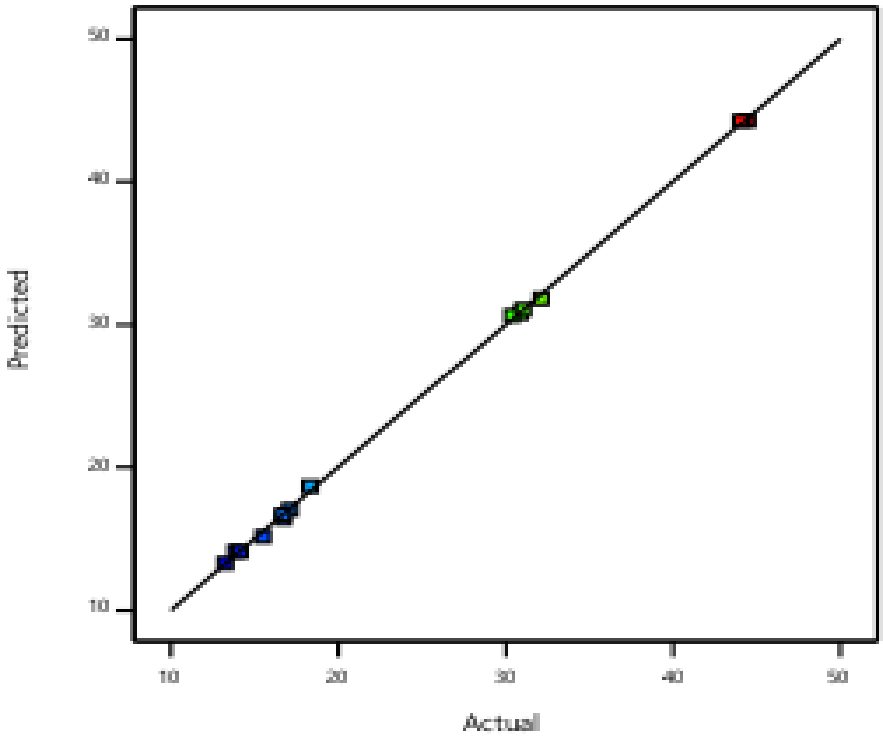

Figure 4. Correlation between experimental and predicted yield of carbon product over different variables derived from RSM model.

Preprints (www.preprints.org) | NOT PEER-REVIEWED | Posted: 11 June 2021 doi:10.20944/preprints202106.0325.v1

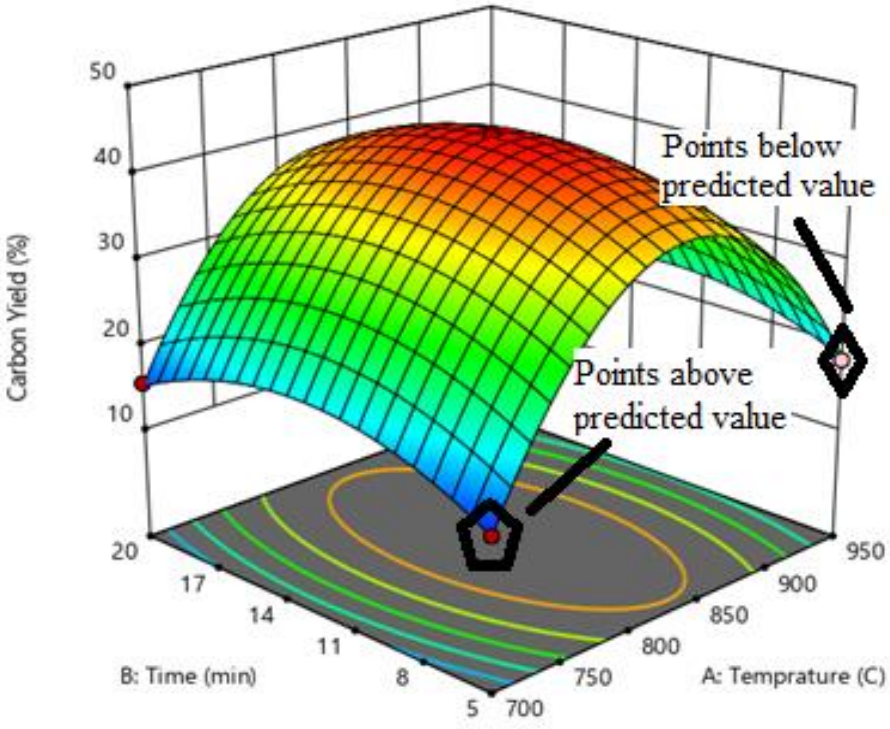

Figure 5. Three-dimensional response plot showing the effect of variables over the carbon yield.

3.4 Effect of temperature on growth of CNTs

To investigate the effect of temperature on the carbon yield a three-dimensional response surface curve figure. 6 was used. Curves were obtained to assess the effect of independent variables and their interactive effect on the carbon yield. The carbon yield was found maximum with the catalyst load of 100mg at around 800-900°C. However, at high temperatures from 850 to 900°C, vapors of hydrocarbon pass out of the crucible quickly, which causes a reduction in the hydrocarbon source for CNT growth.

Preprints (www.preprints.org) | NOT PEER-REVIEWED | Posted: 11 June 2021 doi:10.20944/preprints202106.0325.v1

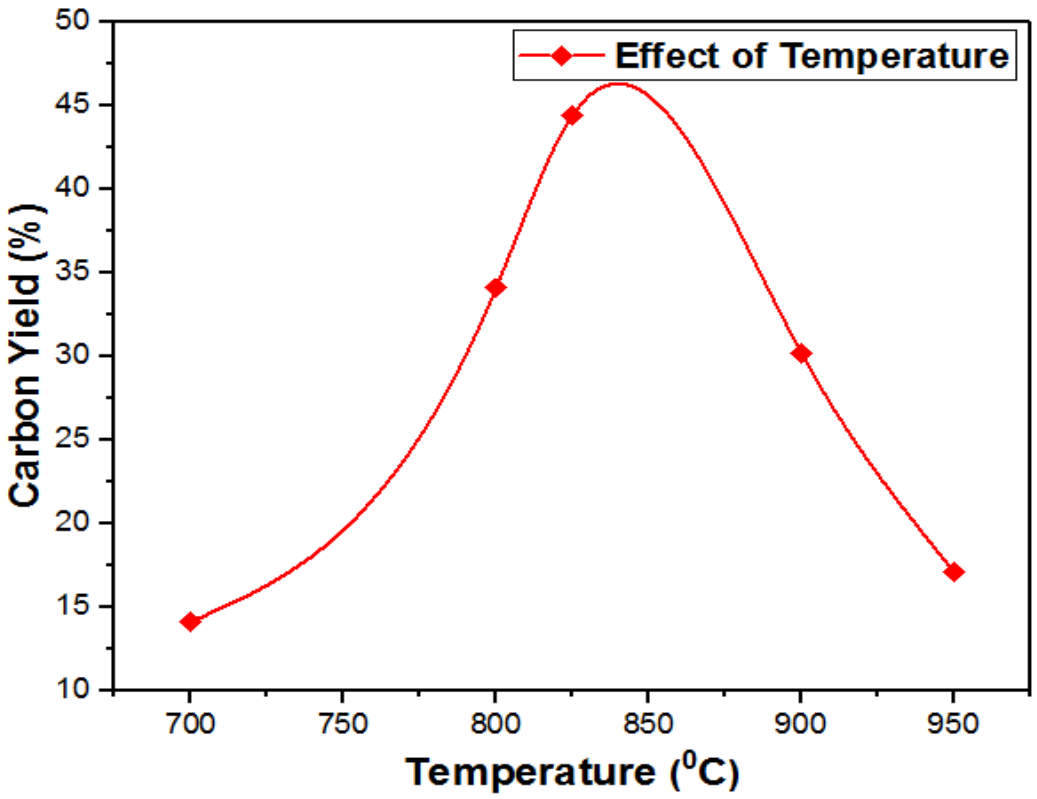

Figure 6. Effect of optimized temperature on carbon yield.

3.5 Effect of reaction time on CNTs growth

The effect of reaction time on the CNTs yield is shown in figure 7. In all experiments, the poultry waste weight (4g) was kept constant. It was observed that CNTs yield was continuously decreased as the reaction time within the tube furnace was increased. It was also observed that only for 10-12 min the hydrocarbon vapors remain in contact with catalyst particles and then the carbon-rich vapors start passing out from the porcelain boat. When the samples were exposed to a higher temperature for a longer time it resulted from the oxidation of hydrocarbons which was the major cause reduction in CNTs yield [36].

Preprints (www.preprints.org) | NOT PEER-REVIEWED | Posted: 11 June 2021 doi:10.20944/preprints202106.0325.v1

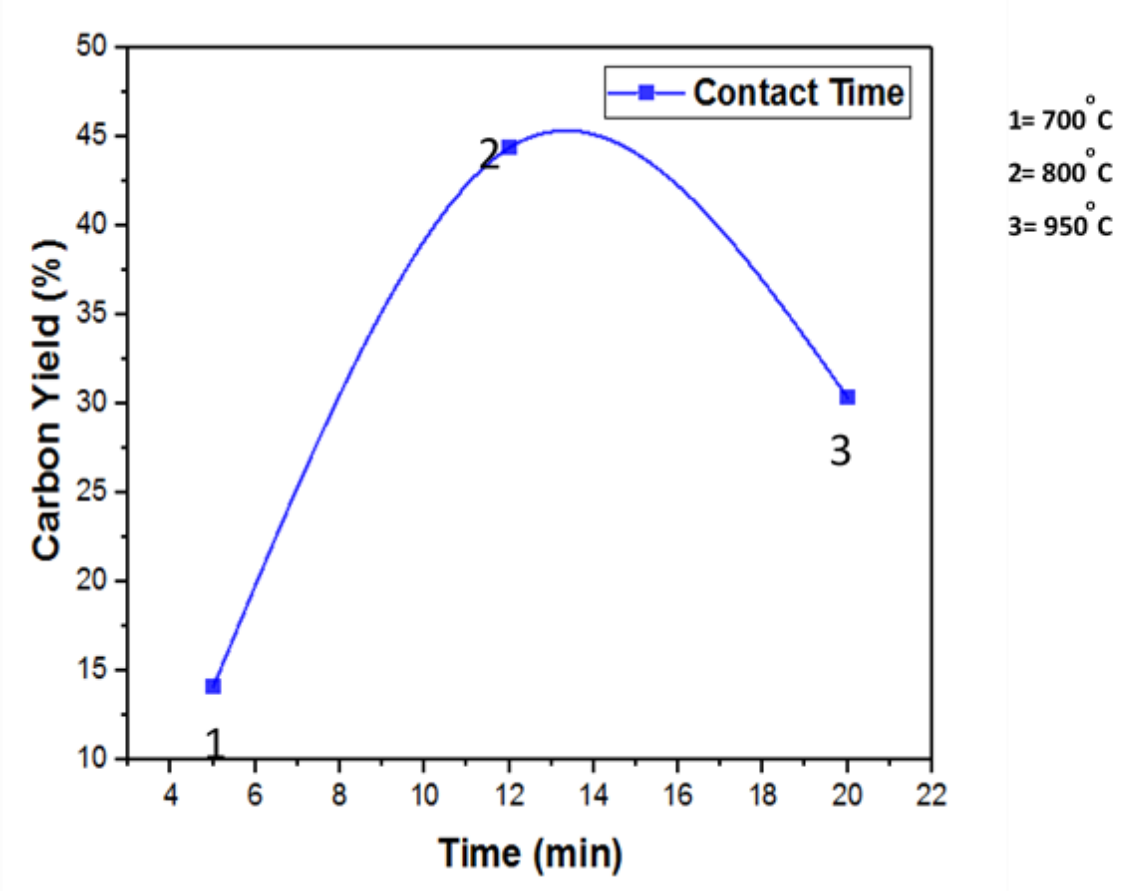

Figure 7. Effect of optimized contact time on carbon yield.

3.6 Characterization of Catalyst

3.6.1 X-ray diffraction (XRD)

The XRD pattern of Ni/Mo/MgO (4: 0.2 :1) catalyst is shown in figure. 8. In these patterns, the intense peaks at 37.30◦ and 43.28◦ correspond to Mg and MoNi respectively. It was confirmed that Ni and Mo particles are well supported over MgO matrix and sintering was not observed due to the presence of sharp peaks [37].

Preprints (www.preprints.org) | NOT PEER-REVIEWED | Posted: 11 June 2021 doi:10.20944/preprints202106.0325.v1

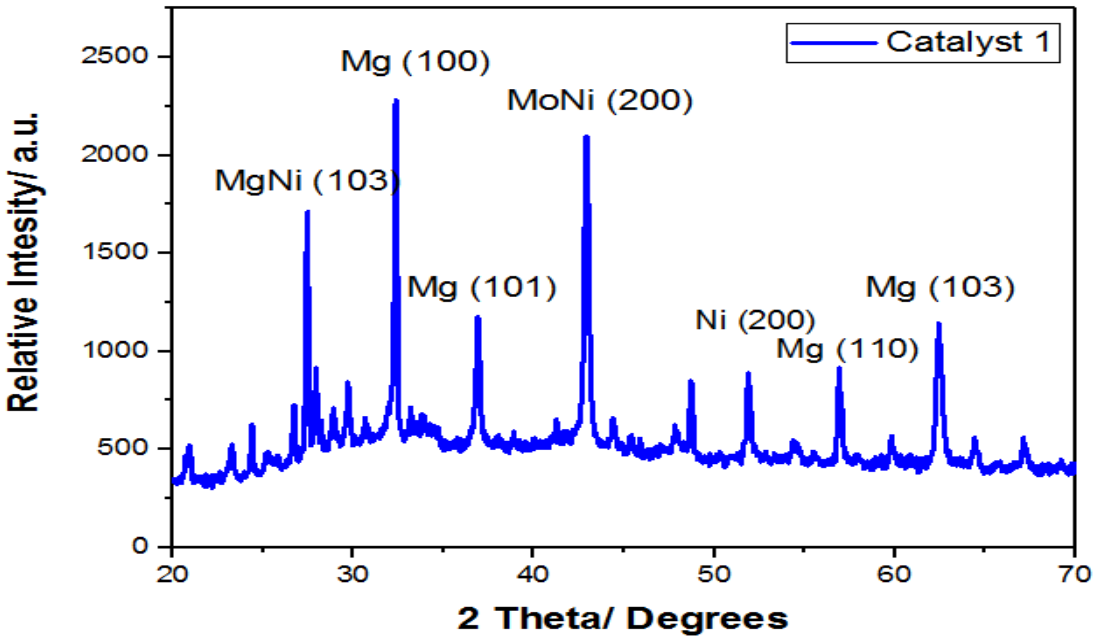

Figure 8. XRD of the optimized molar ratio of Ni/Mo/Mg (4:0.2:1) catalyst.

3.6.2 Morphological analysis of catalyst

Scanning Electron Microscopy (SEM) was used to examine the surface morphologies of various samples. The morphology of Ni/Mo/MgO catalyst at ×100, 000/- magnification is shown in figure 9, at this magnification the particle size is 18 nm. A Uniform catalyst layer with a good distribution of Ni, Mo, and MgO (4:0.2:1) particles were observed from catalyst morphology. The metal particles were appeared in individual crystals as well as in segregated form. Due to the dark and spherical shape of both Ni and Mo It was difficult to differentiate the Ni and Mo particles as shown in figure 9. Ni and Mo particles are well incorporated in the Mg matrix as shown from the microstructure of the Ni/Mo/MgO. Various Mg–Mo and Ni–Mo phases for Ni/Mo/MgO catalyst were shown by the XRD report therefore these results are in agreement with XRD.

Preprints (www.preprints.org) | NOT PEER-REVIEWED | Posted: 11 June 2021 doi:10.20944/preprints202106.0325.v1

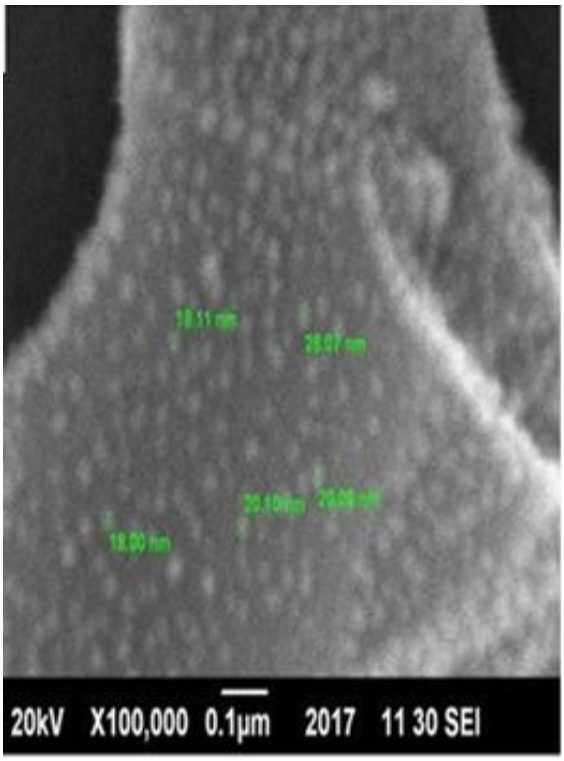

Figure 9. SEM of the catalyst with the ratio of Ni_4 $Mo_{0.1}MgO_1$.

3.7 Characterization of CNTs

XRD, SEM and HRTEM techniques were used to study the highest and lowest effects over the CNTs yield with the different mole ratio of Ni/Mo/MgO catalyst.

3.7.1 X-ray diffraction (XRD)

The XRD patterns of synthesized CNTs over 0.1g of Ni/Mo/MgO catalyst at 825°C, combustion time of 12 min, and 4g of poultry litter is shown in figure 10. The well-resolved graphite (0 0 2) peak at 2θ = 26.62◦ was observed which indicates the growth of CNTs. During the synthesis of CNTs, the diffusion of carbon into Mo and Ni nanoparticles occurs and Mo gets converted to a Mo carbide phase (MoC and Mo_2C) [34]. Carbon nanotube bundles are formed due to the precipitation of carbon atoms that takes place on Ni–Mo crystal plane. Precipitation of carbon atoms on the surface of the catalyst takes place when more carbon atoms diffuse on Ni and Mo nanoparticles. The XRD pattern for the purified CNT (figure. 10), shows a sharp peak (0 0 2) with high intensity which indicates the absence of amorphous carbon [38]. The peak at 2θ = 44.60◦ is due to the presence of Ni particles in the CNT product. The intensity of this peak was decreased

Preprints (www.preprints.org) | NOT PEER-REVIEWED | Posted: 11 June 2021 doi:10.20944/preprints202106.0325.v1

after purification of CNTs. In the purification step, the partial removals of the catalyst particles through acid treatment was confirmed [39].

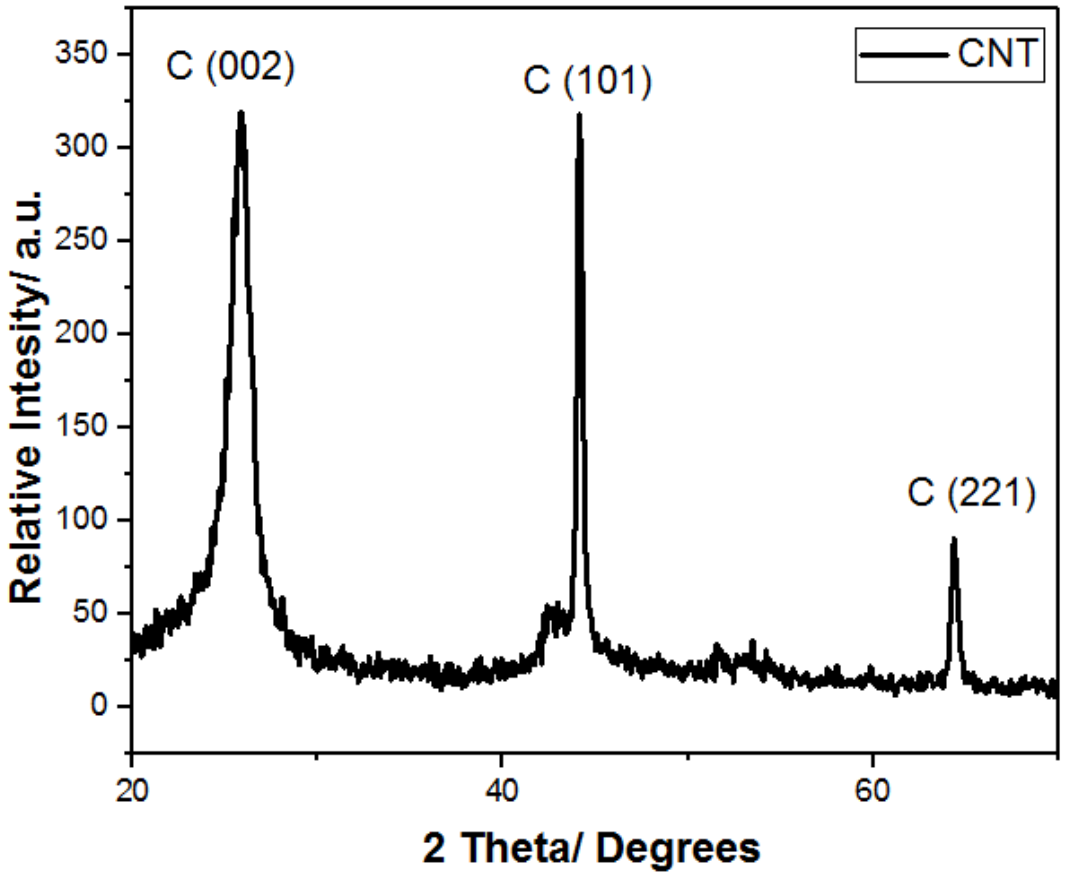

Figure 10. XRD of Synthesized CNTs.

3.7.2 Raman Spectroscopy

Raman spectra results showed two characteristic bands at 1340 ± 5 cm−1 and 1580 ± 5 cm−1 as shown in figure 11. The band at 1340 cm−1 is denoted as D (disorder) mode, which corresponds to the local structural impurities, disorder and defects. The band at 1580 cm−1 is attributed to G (graphite) mode, which corresponds to the degree of graphitization of MWCNTs [40]. A slight shifting of D and G mode for the samples was observed and the peak intensity ratio was found to be 0.85. This lower peak intensity ratio for the purified CNTs was due to the fact of distortion of the graphene layer, which occurs during concentrated HCl treatment.

Preprints (www.preprints.org) | NOT PEER-REVIEWED | Posted: 11 June 2021 doi:10.20944/preprints202106.0325.v1

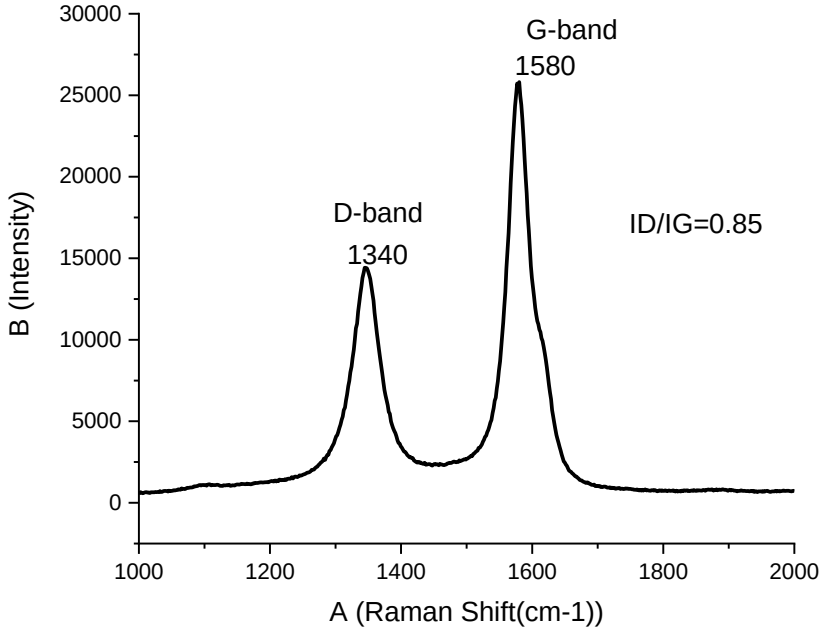

Figure 11. Raman spectra of CNTs synthesize at 825◦C with 12 min combustion time over Ni4Mo0.2MgO1 catalyst.

3.7.3 Morphological Analysis of CNTs

Scanning electron microscopy (SEM) and transmission electron microscopy (TEM) micrographs of synthesized CNTs over Ni/Mo/Mg (4:0.2:1) catalyst is shown in figure 12. It was very difficult to determine the % removal impurity from the SEM image of the purified CNT as it looks like to that of unpurified CNTs. Longer CNTs were produced when the catalyst at the tip of CNTs provides maximum exposure for hydrocarbon [41]. The size of synthesized CNTs at × 75,000 magnifications was 26nm.

A high-resolution transmission electron microscope (HRTEM) was used to characterize the structure and size of nanomaterials. Figure. 13 shows the CNTs obtained at the growth time of 12 min, using the catalyst Ni4Mo0.2MgO1 which is covered by many graphitized layers. These are (a) 200nm MWCNTs with well-aligned graphene walls (b) 100 nm show distorted graphene walls and (c) 50 nm MWCNTs. Thus, the purity and graphitization of CNTs were enhanced during growth time. The TEM images of purified MWCNTs in which the long intertwined CNTs were

Preprints (www.preprints.org) | NOT PEER-REVIEWED | Posted: 11 June 2021 doi:10.20944/preprints202106.0325.v1

found not much very clean but almost impurities had been removed. Despite purification with acid treatment, the produced CNTs contained minute impurities such as amorphous carbon, fullerenes, and catalyst particles which can be seen as a black spot in the TEM image as shown in figure 13. Thus, the purification for MWCNTs was not much effective in this study, which is a serious issue for CNTs to be directly used as a functional filler in composite materials. TEM observations shows that the most probable diameters of nanotubes are around about 50 nm.

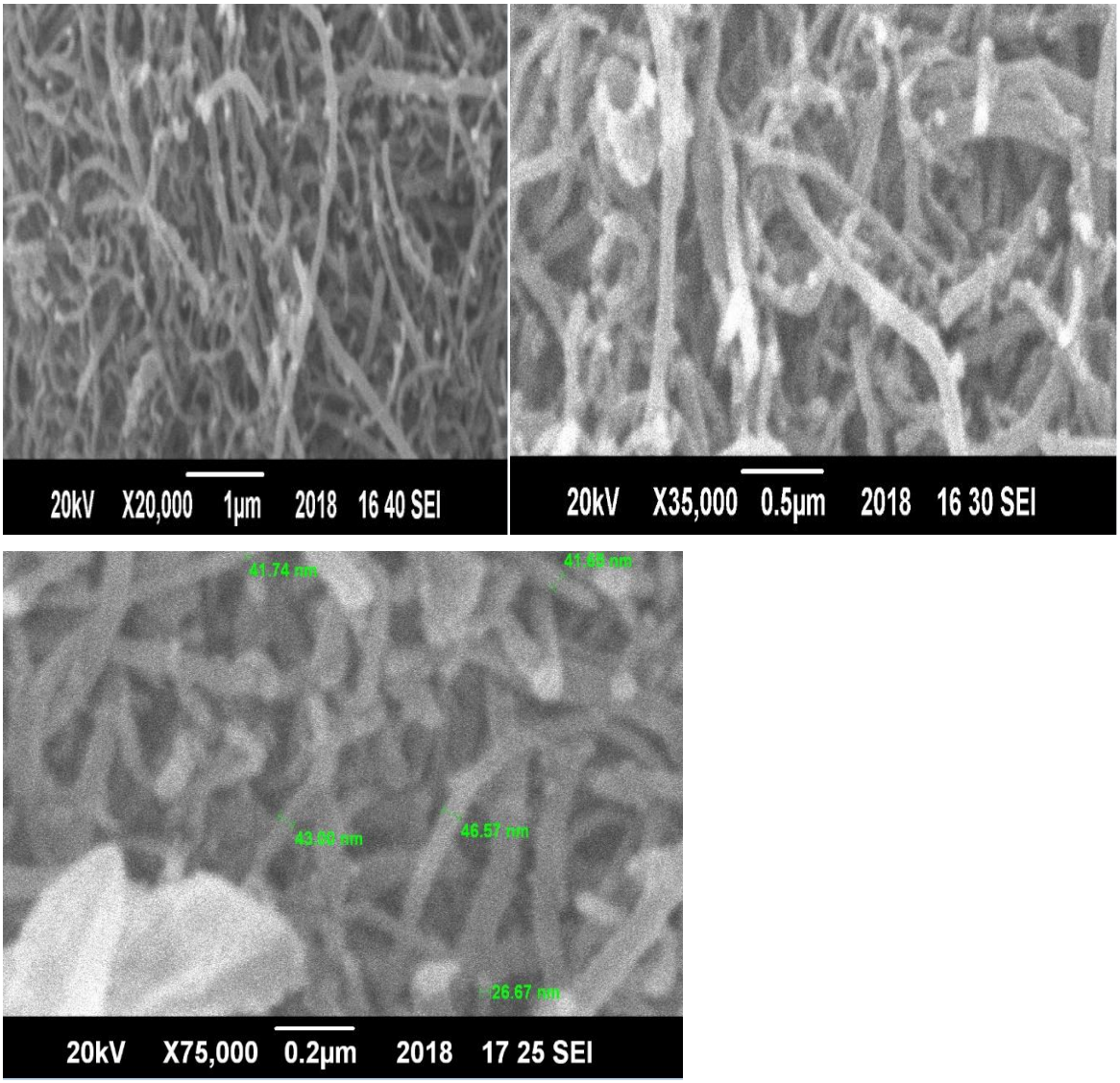

Figure 12. Scanning electron micrographs of synthesized CNTs at different magnifications.

Preprints (www.preprints.org) | NOT PEER-REVIEWED | Posted: 11 June 2021 doi:10.20944/preprints202106.0325.v1

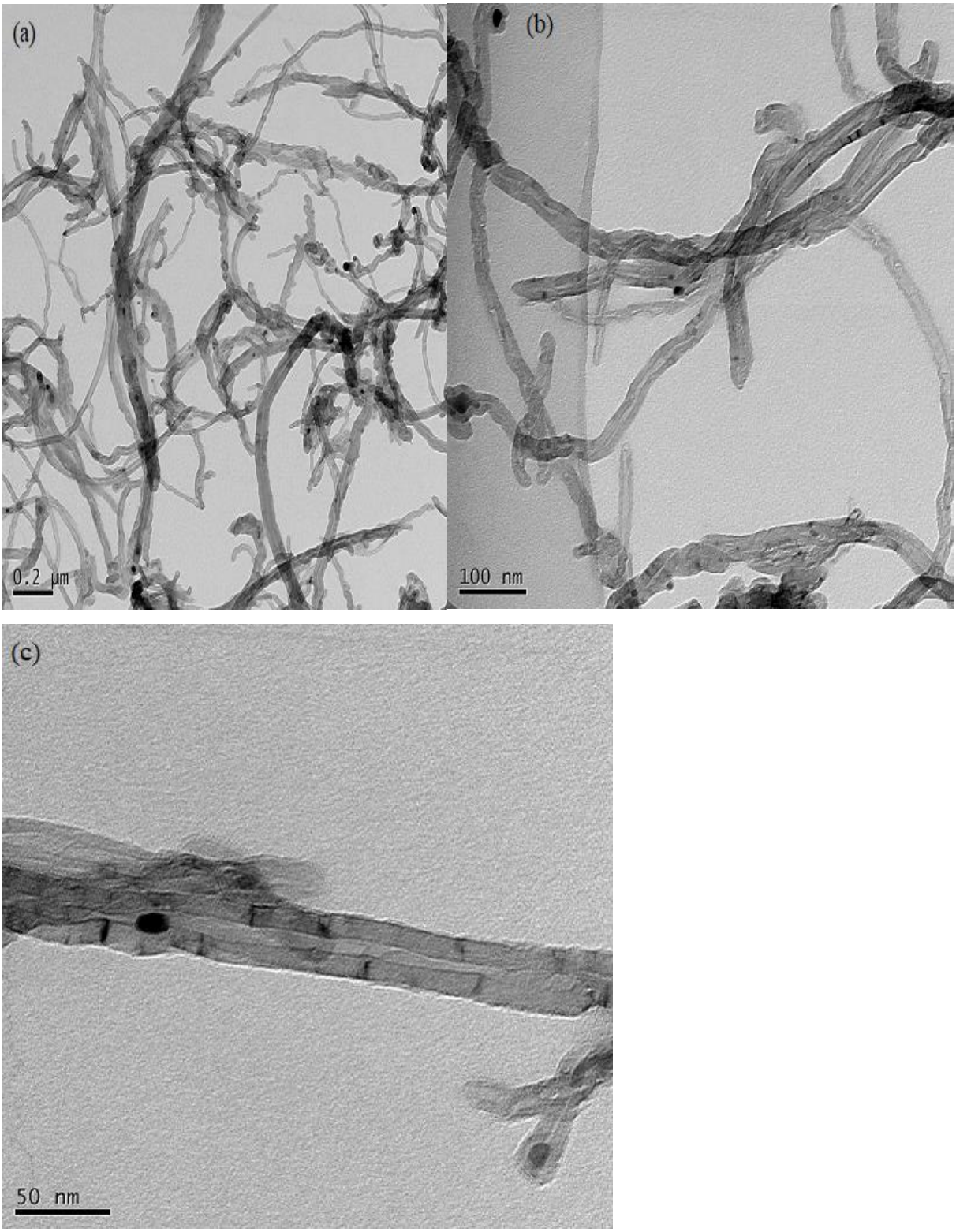

Figure 13. HRTEM images of purified CNTs (a) 0.2µm, (b) 100 nm and (c) 50 nm

Preprints (www.preprints.org) | NOT PEER-REVIEWED | Posted: 11 June 2021 doi:10.20944/preprints202106.0325.v1

3.8 Adsorption of Cr (VI)

Synthesized CNTs were used to remove chromium from synthetic wastewater. 81.83% of Cr (VI) removal was achieved by using MWCNT at pH 3, 400 rpm, and 2.8 hrs. for a dosage of 2-8mg of CNTs. While 78.8% removal of Cr (VI) from wastewater by using MWCNTs has been reported [42]. The outcomes of these studies confirmed that CNTs are an excellent adsorbent for the removal of heavy metal from aqueous solutions.

3.8.1 Effect of pH

For controlling the Cr (VI) adsorption process, system pH was observed as one of the key parameters in this study. The maximum removal efficiency of Cr (VI) was found higher at low pH as shown in figure 14. The optimum pH was observed at pH 3.0 and remaining experiments were done at this pH. As pH increases, the surface of CNTs becomes more negatively charged. This fact causes repulsion between Cr (VI) and CNTs therefore, the removal efficiency decreases with an increase in pH [43]. Different results were obtained with varying pH values and it was confirmed that removal of Cr (VI) by MWCNTs was highly dependent on the pH value of the solution. It was observed that as the pH values increases from 2.0 to 7.0 the adsorption capacity decreases. This observable fact is explained here due to the presence of different forms of Cr (VI) in the aqueous phase. The dominant forms of Cr (VI) were $Cr_2O_7^{-2}$ and $HCrO_4^{-2}$ ions in the pH range of 2 - 7. The surface of MWCNTs became positively charged at low pH values due to protonation effect and thus Cr (VI) adsorption was enhanced due to electrostatic forces between the MWCNTs and the negatively charged $Cr_2O_7^{-2}$ and $HCrO_4^{-2}$ ions [44]. While CrO_4^{-2} ions prevailed in the solution at higher pH values the MWCNTs surface protonation decreases and the adsorption efficiency is thus decreased [45].

Preprints (www.preprints.org) | NOT PEER-REVIEWED | Posted: 11 June 2021 doi:10.20944/preprints202106.0325.v1

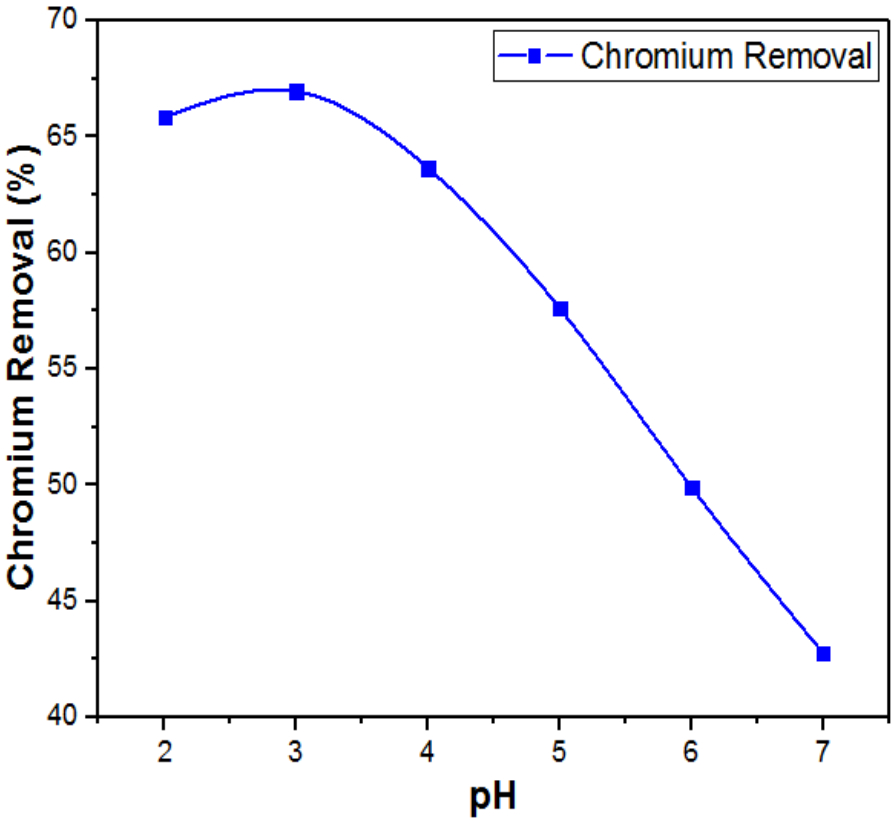

Figure 14. Effects of pH on removal of Cr (VI).

3.8.2 Effect of adsorbent dosage on chromium removal.

As the adsorbent dosage was increased from 2 to 8 mg, keeping all the other parameters constant, the removal of Cr (VI) was observed increasing as shown in figure 15. Highest removal rate was observed at low concentrations of the adsorbent. This is due to the fact that the number of active sites is higher at lower adsorbent concentrations. However, it decreases as the aggregation of particles take place at higher concentration of the adsorbent dosage [46].

Preprints (www.preprints.org) | NOT PEER-REVIEWED | Posted: 11 June 2021 doi:10.20944/preprints202106.0325.v1

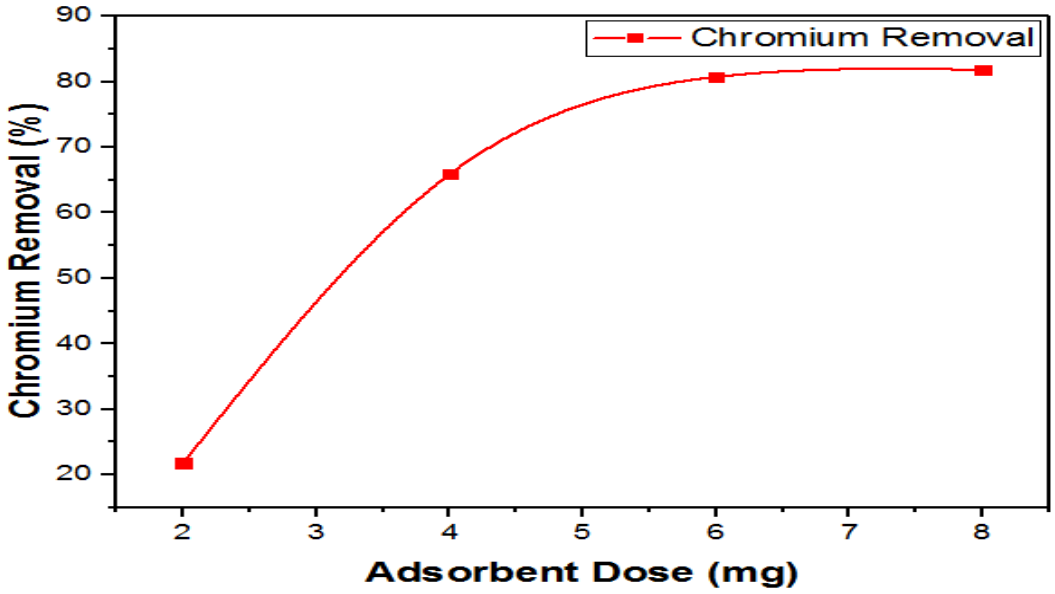

Figure 15. Effects of adsorbent dosage on removal of Cr (VI).

3.8.3 Effect of adsorption contact time.

The removal efficiency of Cr (VI) was increased to 81% as the time of adsorption was studied from 30 to 200 minutes at pH 3 and adsorbent (MWCNTs) dose of 8 mg. The maximum removal was noted at 180 minutes of adsorption time as shown in figure 16 The surface coverage of the adsorbent was higher as time progresses and furthers no adsorption takes place [30].

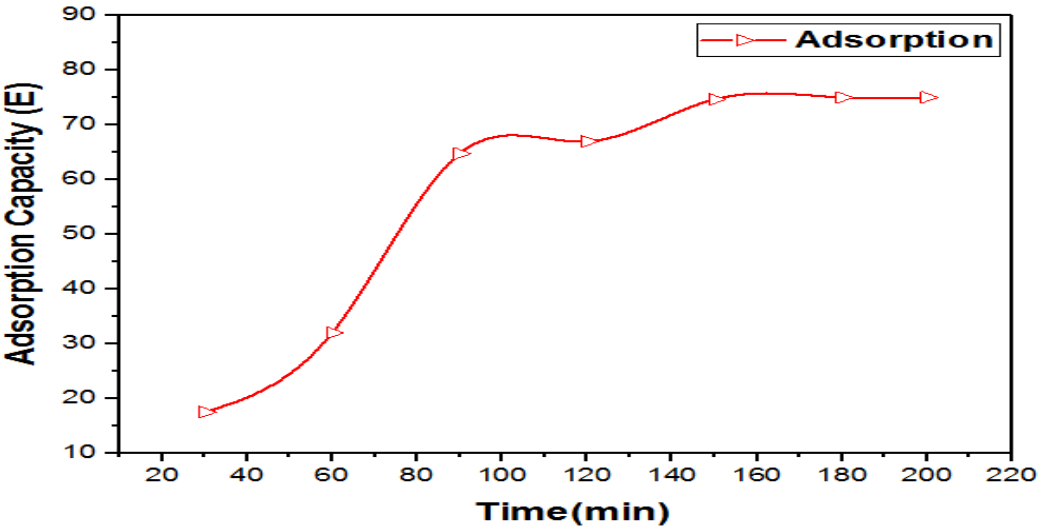

Figure 16. Effect of contact time on the adsorption process.

Preprints (www.preprints.org) | NOT PEER-REVIEWED | Posted: 11 June 2021 doi:10.20944/preprints202106.0325.v1

4 Conclusions

Poultry litter was used as a hydrocarbon source for CNTs production. Response Surface Methodology (RSM) was adopted to optimize Ni/Mo/MgO mole ratio. Among them, the Ni metal was found with the highest proportion as compared to Mo and MgO. Poultry waste as a hydrocarbon source was combusted in the presence of Ni/Mo/MgO catalyst in an electrically heated tube furnace for the growth of CNTs. A high yield of CNTs was obtained using an optimized molar ratio (Ni/Mo/MgO (4:0.2:1) of catalytic precursors at 825^{o}C, 4g poultry litter weight, 100 mg catalyst weight with 12 min of combustion time.

The synthesized CNTs were used in wastewater treatment for the removal of Cr (VI) because MWCNTs exhibited excellent adsorption properties. Adsorption efficiency by MWCNTs was increased with high adsorbent dosage, but the equilibrium adsorption capacity decreased considerably. As the pH value was increased the adsorption capacity was found to decrease. Maximum adsorption of Cr (VI) from synthetic wastewater by synthesized MWCNTs was noted 82.0%.

Acknowledgement

The authors gratefully acknowledge National University of Science and Technology (NUST), Islamabad, Pakistan for providing financial support and facilities required to carry out this work.

Authors contribution: Noor Haleem prepared the main manuscript text, Shahid Nawaz Khan & Dr. Yousuf Jamal help in interpretation of data and in manuscript write up, Dr. Muhammad Anwar Baig & Noor Haleem prepared figures and tables. Dr Yousuf Jamal and Muhammad Anwar Baig are the supervision. All authors have reviewed the manuscript.

Funding: This work was funded by the Institute of Environmental Sciences and Engineering (IESE**), National University of Sciences and Technology (NUST).**

Institutional Review Board Statement: Not applicable.

Informed Consent Statement: Not applicable.

Data Availability Statement: The data presented in this study are available on request from the corresponding author.

Competing interests: The corresponding author certify that they have NO affiliations with any financial interest or non-financial interest with any organization in the subject matter or materials discussed in this manuscript.

References

1. Liaqat, I. **Pakistan poultry industry growth and challenges**. Approach in Poult, Dairy & Veterin Sci. **2018,** *2*, 174-175.

2. Hussain, J.; Rabbani, I.; Aslam, S., Ahmad, H.A. **An overview of poultry industry in Pakistan**. World's Poult. Sci. J. **2015,** *71*, 689-700.

3. Santos Dalólio, F.;da Silva, J.N.;Carneiro de Oliveira, A.C.;Ferreira Tinôco, I.d.F.;Christiam Barbosa, R.;Resende, M.d.O.;Teixeira Albino, L.F., Teixeira Coelho, S. **Poultry litter as biomass energy: A review and future perspectives**. Renewable Sustainable Energy Rev. **2017,** *76*, 941-949.

4. Ali, S.; Ali, S., Riaz, B. **Estimation of Technical Efficiency of Open Shed Broiler Farmers in Punjab, Pakistan: A Stochastic Frontier Analysis** J. Econ Sustainable Dev. **2014,** *5*, 79-88.

5. Leytem, A.B.;Plumstead, P.W.;Maguire, R.O.;Kwanyuen, P.;Burton, J.W., Brake, J. **Interaction of Calcium and Phytate in Broiler Diets. 2. Effects on Total and Soluble Phosphorus Excretion**. Poult. Sci. **2008,** *87*, 459-467.

6. Ullah, I.; Ali, S.; Ullah Khan, S., Sajjad, M. **Assessment of technical efficiency of open shed broiler farms: The case study of Khyber Pakhtunkhwa province Pakistan**. J. Saudi Soc. Agric. Sci. **2019,** 361-366.

7. Singh, A.A., Alhattab, M.K. **Drying poultry manure for pollution potential reduction and production of organic fertilizer**. Am. J. Environ. Sci. **2013,** *9*, 88-102.

8. Jiang, Z.C.a.X. **Microbiological Safety of Chicken Litter or Chicken Litter-Based Organic Fertilizers: A Review**. Agriculture. **2014,** *4*, 1-29.

9. Chan, K.Y.; Van Zwieten, L.; Meszaros, I.; Downie, A., Joseph, S. **Using poultry litter biochars as soil amendments**. Soil Res. **2008,** *46*, 437-444.

10. Lima, I., Marshall, W.E. **Utilization of turkey manure as granular activated carbon: Physical, chemical and adsorptive properties**. Waste Manage. **2005,** *25*, 726-732.

11. Ng, S.W.L.; Yilmaz, G.; Ong, W.L., Ho, G.W. **One-step activation towards spontaneous etching of hollow and hierarchical porous carbon nanospheres for enhanced pollutant adsorption and energy storage**. Appl. Catal., B. **2018,** *220*, 533-541.

12. Kim, S.-W.; Behera, S.K.; Jamal, Y., Park, H.-S. **Optimization of Sodium Hydrosulfide Synthesis for Metal Recovery from Wastewater Using Flue Gas Containing H2S**. J. Environ. Eng. **2016,** *142*, C40150091-C40150097.

13. Khoso, W.A.; Haleem, N.; Baig, M.A., Jamal, Y. **Synthesis, characterization and heavy metal removal efficiency of nickel ferrite nanoparticles (NFN's)**. Sci. Rep. **2021,** *11*, 3790.

14. Hassan, M.M.; Haleem, N.; Baig, M.A., Jamal, Y. **Phytoaccumulation of heavy metals from municipal solid waste leachate using different grasses under hydroponic condition**. Sci. Rep. **2020,** *10*, 15802.

15. Zhong, R., Sels, B.F. **Sulfonated mesoporous carbon and silica-carbon nanocomposites for biomass conversion**. Appl. Catal., B. **2018,** *236*, 518-545.

16. L M Hoyos-Palacio; A G García; J F Pérez-Robles; J González, Martínez-Tejada, H.V. **Catalytic effect of Fe, Ni, Co and Mo on the CNTs production**. IOP Conf. Ser.: Mater. Sci. Eng. **2014,** *59*, 012005.

17. Mamalis, A.G.; Vogtländer, L.O.G., Markopoulos, A. **Nanotechnology and nanostructured materials: trends in carbon nanotubes**. Precis. Eng. **2004,** *28*, 16-30.

18. Zhu, Z.; Chan, Y.-C.; Chen, Z.; Gan, C.-L., Wu, F. **Effect of the size of carbon nanotubes (CNTs) on the microstructure and mechanical strength of CNTs-doped composite Sn0.3Ag0.7Cu-CNTs solder**. Mater. Sci. Eng. A. **2018,** *727*, 160-169.

19. Yao, Y.;Lian, C.;Wu, G.;Hu, Y.;Wei, F.;Yu, M., Wang, S. **Synthesis of "sea urchin"-like carbon nanotubes/porous carbon superstructures derived from waste biomass for treatment of various contaminants**. Appl. Catal., B. **2017,** *219*, 563-571.

20. Tripathi, P.K.; Durbach, S., Coville, N.J. **Synthesis of Multi-Walled Carbon Nanotubes from Plastic Waste Using a Stainless-Steel CVD Reactor as Catalyst**. Nanomaterials **2017,** *7*, 284.

21. Li, Z.; Yu, X.; Liang, Y., Wu, S. **Carbon Nanomaterials for Enhancing the Thermal, Physical and Rheological Properties of Asphalt Binders**. Materials. **2021,** *14*, 2585.

22. Wang, J.; Shen, B.; Lan, M.; Kang, D., Wu, C. **Carbon nanotubes (CNTs) production from catalytic pyrolysis of waste plastics: The influence of catalyst and reaction pressure**. Catal. Today. **2020,** *351*, 50-57.

23. Yang, Y.;Wang, R.;Ding, L.;Qu, D.;Zhang, Y.;Han, Q.;Liu, N., Piao, Y. **Catalytic performance and mechanism of biochars for dechlorination of tetrachloroethylene in sulfide aqueous solution**. Appl. Catal., B. **2020,** *278*, 119285.

24. Melchionna, M.;Beltram, A.;Stopin, A.;Montini, T.;Lodge, R.W.;Khlobystov, A.N.;Bonifazi, D.;Prato, M., Fornasiero, P. **Magnetic shepherding of nanocatalysts through hierarchically-assembled Fe-filled CNTs hybrids**. Appl. Catal., B. **2018,** *227*, 356-365.

25. De Luca, P.; Siciliano, C.; Macario, A., Nagy, J.B. **The Role of Carbon Nanotube Pretreatments in the Adsorption of Benzoic Acid**. Materials. **2021,** *14*, 2118.

26. Jia, Z.;Kou, K.;Qin, M.;Wu, H.;Puleo, F., Liotta, F.L. **Controllable and Large-Scale Synthesis of Carbon Nanostructures: A Review on Bamboo-Like Nanotubes**. Catalysts. **2017,** *7*, 256.

27. Bezerra, M.A.; Santelli, R.E.; Oliveira, E.P.; Villar, L.S., Escaleira, L.A. **Response surface methodology (RSM) as a tool for optimization in analytical chemistry**. Talanta. **2008,** *76*, 965-977.

28. Vivekchand, S.R.C.; Govindaraj, A.; Seikh, M.M., Rao, C.N.R. **New Method of Purification of Carbon Nanotubes Based on Hydrogen Treatment**. J. Phys. Chem. B. **2004,** *108*, 6935-6937.

29. Naseh, M.V.;Khodadadi, A.A.;Mortazavi, Y.;Sahraei, O.A.;Pourfayaz, F., Mosadegh, S. **Functionalization of carbon nanotubes using nitric acid oxidation and DBD plasma**. World Acad Sci. Eng. Technol. **2009,** *49*, 177-179.

30. Anjum, M.; Miandad, R.; Waqas, M.; Gehany, F., Barakat, M.A. **Remediation of wastewater using various nano-materials**. Arabian J. Chem. **2016,** 4897-4919.

31. Zhang, C.;Gong, Y.;Liu, H.;Jin, C.;Guo, H., He, J. **An efficient Co-WN/CNTs composite catalyst with multiple active sites for oxygen reduction reaction activity**. Chem. Phys. Lett. **2021,** *770*, 138452.

32. Modekwe, H.U.; Mamo, M.; Moothi, K., Daramola, M.O. **Synthesis of bimetallic NiMo/MgO catalyst for catalytic conversion of waste plastics (polypropylene) to carbon nanotubes (CNTs) via chemical vapour deposition method**. Mater. Today: Proc. **2021,** *38*, 549-552.

33. Memon, I.N.; Kumbhar, M.I., Noonari, S. **Economics of Poultry Waste Use as a Fertilizer in Sindh Pakistan**. J Fisheries Livest Prod. **2016,** 1-9.

34. Bajad, G.S.; Tiwari, S.K., Vijayakumar, R.P. **Synthesis and characterization of CNTs using polypropylene waste as precursor**. Mater. Sci. Eng. B. **2015,** *194*, 68-77.

35. Şahan, T., Öztürk, D. **Investigation of Pb(II) adsorption onto pumice samples: application of optimization method based on fractional factorial design and response surface methodology**. Clean Technol. Environ. Policy. **2014,** *16*, 819-831.

36. Arena, U.; Mastellone, M.L., Perugini, F. **The environmental performance of alternative solid waste management options: a life cycle assessment study**. Chem. Eng. J. **2003,** *96*, 207-222.

37. Silva-Rodrigo, R.;Hernández-López, F.;Martinez-Juarez, K.;Castillo-Mares, A.;Melo Banda, J.A.;Olivas-Sarabia, A.;Ancheyta, J., Rana, M.S. **Synthesis, characterization and catalytic properties of NiMo/Al2O3–MCM-41 catalyst for dibenzothiophene hydrodesulfurization**. Catal. Today. **2008,** *130*, 309-319.

38. Stamatin, I.;Morozan, A.;Dumitru, A.;Ciupina, V.;Prodan, G.;Niewolski, J., Figiel, H. **The synthesis of multi-walled carbon nanotubes (MWNTs) by catalytic pyrolysis of the phenol-formaldehyde resins**. Phys. E. **2007,** *37*, 44-48.

39. Das, R.; Abd Hamid, S.B.; Ali, M.; Ramakrishna, S., Yongzhi, W. **Carbon Nanotubes Characterization by X-ray Powder Diffraction – A Review**. Curr. Nanosci. **2015,** *11*,

40. Saad, N.A.; Ramya, E.; Saikiran, V.; Naraharisetty, S.R.G., Narayana Rao, D. **Novel synthesis and study of nonlinear absorption and surface-enhanced Raman scattering of carbon nanotubes decorated with silver nanoparticles**. Chem. Phys. **2020,** *533*, 110703.

41. Safarova, K.; Dvorak, A.; Kubinek, R.; Vujtek, M., Rek, A. Usage of AFM, SEM and TEM for the research of carbon nanotubes. In *Modern Research and Educational Topics in Microscopy.* , Méndez-Vilas, A.; Díaz, J. (eds.) (2007), Vol. 1, pp 513-519. http://citeseerx.ist.psu.edu/viewdoc/download?doi=10.1.1.618.9072&rep=rep1&type=pdf

42. Burakov, A.E.; Burakova, I.V.; Galunin, E.V., Kucherova, A.E. New Carbon Nanomaterials for Water Purification from Heavy Metals. In *Handbook of Ecomaterials*, Martínez, L. M. T.; Kharissova, O. V.; Kharisov, B. I. (eds.) Springer International Publishing, Cham, (2019), pp 1-20. https://doi.org/10.1007/978-3-319-68255-6_166

43. Jiang, W.;Pelaez, M.;Dionysiou, D.D.;Entezari, M.H.;Tsoutsou, D., O'Shea, K. **Chromium(VI) removal by maghemite nanoparticles**. Chem. Eng. J. **2013,** *222*, 527-533.

44. Li, Z., Bowman, R.S. **Retention of inorganic oxyanions by organo-kaolinite**. Water Res. **2001,** *35*, 3771-3776.

45. Padmavathy, K.S.; Madhu, G., Haseena, P.V. **A study on Effects of pH, Adsorbent Dosage, Time, Initial Concentration and Adsorption Isotherm Study for the Removal of Hexavalent Chromium (Cr (VI)) from Wastewater by Magnetite Nanoparticles**. Procedia Eng. **2016,** *24*, 585-594.

46. Li, Y.H.;Zhao, Y.M.;Hu, W.B.;Ahmad, I.;Zhu, Y.Q.;Peng, X.J., Luan, Z.K. **Carbon nanotubes - the promising adsorbent in wastewater treatment**. J. Phys.: Conf. Ser. **2007,** *61*, 698-702.

Figure captions

Figure 1. EDS of poultry litter through SEM.

Figure 2. Correlation between experimental and predicted yield of carbon product derived from RSM model.

Figure 3. Three-dimensional response plot showing catalytic activity of Ni, Mo and MgO over the carbon yield.

Figure 4. Correlation between experimental and predicted yield of carbon product over different variables derived from RSM model.

Figure 5. Three-dimensional response plot showing the effect of variables over the carbon yield.

Figure 6. Effect of optimized temperature on carbon yield.

Figure 7. Effect of optimized contact time on carbon yield.

Figure 8. XRD of the optimized molar ratio of Ni/Mo/Mg (4:0.2:1) catalyst.

Figure 9. SEM of the catalyst with the ratio of Ni_4 $Mo_{0.1}MgO_1$.

Figure 10. XRD of Synthesized CNTs.

Figure 11. Raman spectra of CNTs synthesize at 825◦C with 12 min combustion time over Ni4Mo0.2MgO1 catalyst.

Figure 12. Scanning electron micrographs of synthesized CNTs at different magnifications.

Figure 13. HRTEM images of purified CNTs.

Figure 14. Effects of pH on removal of Cr (VI).

Figure 15. Effects of adsorbent dosage on removal of Cr (VI).

 doi:10.20944/preprints202106.0325.v1

Figure 16. Effect of contact time on the adsorption process.